



Published in final edited form as:

*J Immunol.* 2019 August 01; 203(3): 686–695. doi:10.4049/jimmunol.1801540.

## Identification of an intronic regulatory element necessary for tissue-specific expression of *Foxn1* in thymic epithelial cells

Brian M. Larsen<sup>\*</sup>, Jennifer E. Cowan<sup>\*</sup>, Yueqiang Wang<sup>†</sup>, Yu Tanaka<sup>#</sup>, Yongge Zhao<sup>\*</sup>, Benjamin Voisin<sup>‡</sup>, Michael G. Constantinides<sup>§</sup>, Keisuke Nagao<sup>‡</sup>, Yasmine Belkaid<sup>§</sup>, Parirokh Awasthi<sup>¶</sup>, Yousuke Takahama<sup>#</sup>, Avinash Bhandoola<sup>\*</sup>

<sup>\*</sup>Laboratory of Genome Integrity, Center for Cancer Research, National Cancer Institute, National Institutes of Health, Bethesda, MD 20892, USA.

<sup>†</sup>BGI Genomics, BGI-Shenzhen, Shenzhen 518083, China

<sup>#</sup>Experimental Immunology Branch, National Cancer Institute, National Institutes of Health, Bethesda, Maryland 20892, USA

<sup>‡</sup>Dermatology Branch, National Institute of Arthritis and Musculoskeletal and Skin Diseases, National Institutes of Health, Bethesda, MD 20892, USA.

<sup>§</sup>Metaorganism Immunity Section, Laboratory of Immune System Biology, National Institute of Allergy and Infectious Diseases, National Institutes of Health, Bethesda, MD 20892, USA.

<sup>¶</sup>Laboratory Animal Sciences Program, Leidos Biomedical Research Inc., Frederick National Laboratory for Cancer Research, National Institutes of Health, Frederick, MD 21701, USA.

### Abstract

The thymus is critical for the establishment of the adaptive immune system and the development of a diverse T cell repertoire. T cell development depends upon cell-cell interactions with epithelial cells in the thymus. The thymus is composed of two different types of epithelial cells; cortical and medullary epithelial cells. Both of these express, and critically depend on, the transcription factor *Foxn1*. *Foxn1* is also expressed in the hair follicle, and disruption of *Foxn1* function in mice results in severe thymic developmental defects and the hairless (*nude*) phenotype. Despite its importance, little is known about the direct regulation of *Foxn1* expression. In this study, we identify a *cis*-regulatory element critical for expression of *Foxn1* in mouse thymic epithelial cells, but dispensable for expression in hair follicles. Analysis of chromatin accessibility, histone modifications, and sequence conservation identified regions within the first intron of *Foxn1* that possessed the characteristics of regulatory elements. Systematic knockout of candidate regions lead us to identify a 1.6kb region that, when deleted, results in a near total disruption of thymus development. Interestingly, *Foxn1* expression and function in the hair follicle were unaffected. RNA-FISH showed a near complete loss of *Foxn1* mRNA expression in the embryonic thymic bud. Our studies have identified a genomic regulatory element with thymic-specific control of *Foxn1* gene expression.

## Introduction

The thymus is essential for T cell development. The thymus recruits lymphoid progenitors from the bone marrow that settle within the thymus and give rise to T cell progeny. T cell development requires interactions of T cell precursors with multiple cell types, including dendritic and epithelial cells. Two thymic epithelial cell (TEC) subsets play distinct roles in T cell development (1–6). Interactions with cortical TEC (cTEC) result in positive selection, after which selected T cell precursors migrate to the medulla. Subsequently, high affinity interactions with self-peptide processed and presented by medullary TEC (mTEC) or presented by dendritic cells mediate negative selection or differentiation into regulatory T cells (Tregs) (5, 7). This critical process prevents the development of self-reactive T cells that would result in autoimmune syndromes. Naïve T cells that pass both positive and negative selection emigrate from the thymus into the periphery to protect the host. A fully formed and functional thymus and its TEC compartments are therefore critical to the development of a self-tolerant and diverse T cell repertoire.

*Foxn1* was first discovered by a spontaneous mutation in the third exon of *Foxn1* resulting in the *nude* mouse (8, 9). *Foxn1* is expressed in the hair follicle and in TEC and, consequently, the *nude* mouse is hairless and possesses a rudimentary thymus that is non-functional (10, 11). The thymus is endodermally derived and arises from the third pharyngeal pouch. *Foxn1* expression initiates as early as E9.5 in the third pharyngeal pouch in the mouse embryo and precedes the differentiation of the thymus epithelium (8). Both TEC types derive from a common bipotent progenitor (12, 13). While these progenitor cells are maintained in the *nude* mouse, differentiation of these precursor cells into the cTEC and mTEC lineage is blocked (13, 14).

*Foxn1* is important postnatally for the maintenance of thymus function. *Foxn1* is not only critical for the expansion and differentiation of TEC, but also for inducing and maintaining the expression of genes critical for the development of T cells, including *Dll4*, *Cxcl12*, and *Ccl25* (15). Declining *Foxn1* expression is thought to contribute to thymic involution; the age-related reduction of thymus size and the reduction of naïve T cell output (16–19). Postnatal expression of *Foxn1* is critical for the maintenance of TEC, and overexpression in older mice can reverse age-related thymic involution (16, 17, 20, 21). Mutations in the human *FOXN1* gene result in similar phenotypes wherein the patient exhibits congenital alopecia and severe combined immunodeficiency syndrome (22). Study of the regulation of *Foxn1* expression is therefore important to the identification of disease-related variants in humans, and as a way to further understand the loss of TEC populations with age, leading to the decline of thymus function.

Gene regulation is controlled by both proximal and distal cis-regulatory elements (REs). Active genomic REs can be characterized by histone modifications including acetylated lysine 27 of histone 3 (H3K27ac), methylated lysine 4 of histone 3 (H3K4me1), and chromatin accessibility (23, 24). These elements are also highly conserved (25). Through the examination of chromatin characteristics consistent with active REs, we have identified a highly conserved 1.6kb region of the 14.5kb first intron of *Foxn1* that is absolutely critical for *Foxn1* expression in TECs. Deletion of this element results in the complete abrogation of

thymus development and T cell development. Interestingly, this region is not required for hair morphogenesis and *Foxn1* expression in keratinocytes is unaffected. We have therefore identified the first thymus-specific RE essential for expression of *Foxn1* in TEC.

## Materials and Methods

### Mice

*Nude* mice were purchased from The Jackson Laboratory (Stock No: 000819). gRNAs used to generate the RE knockout mice were designed using the [crispr.mit.edu](https://crispr.mit.edu) website. The injection strategy to generate each mutant mouse is outlined in Figure S4B. The gRNA targeting sequence (Fig. S4C) was cloned into a plasmid containing the full gRNA backbone and T7 promoter. gRNAs were transcribed using the MEGAshortscript T7 Transcription Kit (ThermoFisher Scientific). Microinjections to generate knockout mice by CRISPR-Cas9 were performed by the Transgenics/Cryopreservation – Laboratory Animal Sciences Program NCI core on a C57BL/6NCr background. The genomic coordinates of each deletion are provided in Figure S4D.

Mice used in flow cytometry experiments were 4–8 weeks old and of either sex. The ages of embryonic mice are specified with E0.5 being noon of the day of the discovered plug. Animal procedures were approved by relevant National Institutes of Health Animal Care and Use Committees.

### Tissue preparation

Thymus and spleen were dissected into RPMI (ThermoFisher Scientific) containing 5% NCS (Atlanta Biologicals) and mechanically teased with forceps to acquire a single-cell suspension. Splenocytes were treated with ACK Lysing Buffer (Lonza) for 3 minutes on ice to eliminate red blood cells. When analyzing thymic epithelial cells, single-cell thymic suspensions were enzymatically digested with Liberase TM (63ug/ml; Roche) and DNase I (20ug/ml; Roche) for 40 minutes shaking at 37°C. Following digestion, epithelial cells were enriched by centrifugation in a Percoll (GE) gradient. The cell suspensions were then further processed and stained as described below.

Epidermal cell suspensions were prepared from mouse back skin. Hairs were shaved, and skin samples were placed in PBS on ice. After mechanically removing subcutaneous tissue, samples were floated on 10 ml of 0.15% trypsin and 0.75 mM EDTA (a mixture of 5 ml of 0.25% Trypsin-1mM EDTA and 5 ml of 0.05% Trypsin-0.5mM EDTA) (Gibco) and were incubated at 37°C for 45 minutes. The epidermis was then gently scraped off with forceps into PBS containing 2% FBS. Cell suspensions were further mechanically dissociated with a 50 ml syringe (Covidien) and then filtered through a sterile 100 µm cell strainer (BD). The cells were washed with PBS containing 2% FBS and filtered through a 40 µm cell strainer into a new 50 ml conical tube. Hair follicles in anagen phase penetrate through the dermal layer and extend into the hypodermis and can be macroscopically identified from the hypodermal side of the skin. Growing portions of anagen hair follicles were dissected out with scissors and incubated for 30 minutes in a mixture of 0.15% trypsin, 0.75 mM EDTA and 1 mg/mL of Liberase TM (Roche).

Livers were mechanically dissociated through 70  $\mu\text{m}$  filters and centrifuged at 400 g for 5 minutes. Following aspiration of the supernatant, the pellet was resuspended in 10 ml of 37.5% Percoll and then centrifuged at 800 g for 10 minutes. The supernatant was aspirated and the cells were resuspended in complete RPMI containing 10% FBS.

For the isolation of lung lymphocytes, pairs of lungs were diced with a razor blade and incubated in 2 ml of pre-warmed RPMI containing 0.05% DNase I (Sigma) and 0.2% collagenase IV (Sigma) in a 37°C water bath for 20 minutes. The digested tissue was passed through a 70  $\mu\text{m}$  filter and centrifuged at 400 g for 5 minutes. The cells were resuspended in 5 ml of 37.5% Percoll and centrifuged at 800 g for 10 minutes. The supernatant was aspirated and the cells were resuspended in complete RPMI containing 10% FBS. The cell suspensions were then further processed and stained as described below.

### Flow cytometry

Thymocyte and splenocyte cell suspensions were incubated with a mix of purified rat, mouse, and hamster IgG before addition of specific antibodies. Thymocytes and splenocytes were stained and analyzed in FACS buffer (PBS containing 0.1% sodium azide, 1 mM EDTA, and 0.5% BSA). Thymic epithelial cell preps were analyzed in MACS buffer (PBS containing 2 mM EDTA and 0.5% FCS). Antibodies specific for Kit (2B8), CD25 (PC61.5), CD45.2 (104), CD4 (GK1.5), CD8 $\alpha$  (53–6.72), TCR $\beta$  (H57), Ly51 (6C3), EpCAM (G8.8), CD80 (16–10A1), MHCII (M5/114.15.2), were from eBioscience. Biotinylated UEA-1 (B-1065) was from Vector Labs, and Streptavidin (25–4317-82) was from Invitrogen. Thymocyte lineage cocktail was a mix of the following antibodies from eBioscience: B220 (RA3–6B2), CD19 (1D3), Mac-1 (M1/70), Gr-1 (8C5), CD11c (N418), Ter119 (TER119), and NK1.1 (PK136). Splenocyte lineage cocktail was the same as thymocyte but did not include antibodies against CD19 or B220. For intracellular staining, cells were first stained for cell surface molecules, permeabilized using the eBioscience's transcription factor staining buffer set (cat: 00–5523-00) according to the manufacturer's instructions and then stained with antibodies specific to Aire (5H12) or FoxP3 (FJK-16s).

Epidermal cell suspensions harvested from telogen skin were stained with antibodies against CD45.2 (104), EpCAM (G8.8), Sca-1 (D7), and CD34 (RAM34). CD45-Sca-1-EpCAM+ cells contain keratinocytes from the isthmus and bulge and excludes those from the interfollicular epidermis and infundibulum. Anagen cell suspensions were sorted based on the same cell-surface phenotype.

Liver and lung cell suspensions were stained with Thy1.2, CD45.2 (104), TCR $\gamma\delta$  (GL3), TCR $\beta$  (H57), ROR $\gamma\text{t}$ , mMR1 5-OP-RU tetramer, mCD1d PBS57 tetramer, TCR V $\gamma$ 4 (UC3–10A6), and TCR V $\gamma$ 6 (17D1).

Samples were acquired on either a BD LSRFortessa or BD CantoII and analyzed using FlowJo software (Tree Star). Cells were sorted using a BD FACSAria flow cytometer. Absolute cell numbers were calculated using a BD Accuri C6 PLUS flow cytometer.

## ATAC-Seq

ATAC-Seq was performed as described previously (26) with minor modifications. Cells were sorted, and 50,000 cells were pelleted (500 g, 4°C) and washed with PBS followed by incubation in 50 µl of cold lysis buffer (10 mM TRIS-HCl, pH 7.4, 10 mM NaCl, 3 mM MgCl<sub>2</sub>, 0.1% Igepal CA-630) for 15 minutes while centrifuging (500 g, 4°C). Pelleted nuclei were resuspended in transposition reaction mix with Tn5 Transposase (Illumina FC-121–1030) and incubated for 45 minutes with gentle shaking at 37°C. Tagmented DNA was purified using SPRIselect beads (Beckman Coulter B23317) and amplified by PCR. Resulting libraries were size-selected and purified again by SPRIselect beads. Libraries were sequenced by single-read (75 cycles) or paired-end (150 cycles), on the Illumina NextSeq Series System.

Reads were trimmed to remove adapters, sequencing primers or any such unwanted sequences. Trimmed reads were aligned to mm10 blacklisted regions and only reads not aligning to the blacklisted regions were included for further analysis. These reads were aligned to mm10 genome using bowtie2 aligner to generate a BAM alignment file. Duplicates arising due to PCR artifacts were marked and removed using Picardtools package from the Broad Institute. Custom R scripts were run to correct for differences in sequencing depths across samples applying Cyclic Loess normalization. Resulting normalized bed files were used to call peaks using macs2 with ENCODE recommended parameters for ATAC-Seq data. ATAC-Seq data is accessible <https://www.ncbi.nlm.nih.gov/geo/query/acc.cgi?acc=GSE131595>. Transcription factor binding motifs located in peaks indicating open chromatin were annotated using HOMER (27).

## qRT-PCR

Tissue was flash frozen and stored at –80°C until RNA was extracted using a Qiagen RNeasy Mini or Micro Extraction kit depending on cell quantity. Reverse transcription was performed using the SuperScript VILO cDNA Synthesis Kit (Invitrogen). qPCR was performed on a StepOnePlus Real-Time PCR System (Applied Biosystems) using Taqman probes designed against *Foxn1* (Mm00433948; Applied Biosystems) and *Gapdh* (Mm99999915; Applied Biosystems). Results were analyzed using the  $\Delta\Delta C_T$  method.

## RNA-Scope

Embryos were dissected at the indicated ages and fixed in freshly prepared 4% PFA for 24–36 hours at room temperature and then processed into paraffin blocks. Embryos were faced until the thymic bud was visible, and then 5 micron sections were cut serially and mounted onto positively charged glass microscope slides. Slides were stained with the RNAScope® Multiplex Fluorescent V2 Assay (ACDBio.) following the manufacturer's instructions with 30 minute incubations for both the Target Retrieval and Protease Plus digestion steps. Embryo sections were hybridized with either RNAScope 3-plex negative control (320871; ACDBio.), 3-plex positive-Mm control probe (320881; ACDBio.), or *Foxn1*-Mm probes (482021-C2; ACDBio.). Slide images were acquired at a 20X magnification using an Aperio FL scanner.

## Thymus section analysis

Thymus tissues were fixed with 4% (g/vol) PFA and embedded in OCT compound (Sakura Finetek). Frozen thymuses were sliced into 10 micron thick sections and stained with eFluor660-conjugated anti-Aire antibody (Invitrogen, clone 5H12) and rabbit antibody specific for beta5t (28) followed by AlexaFluor488-conjugated anti-rabbit IgG antibody (Invitrogen). Sections were also stained for the reactivity with UEA-1 (Vector Laboratories). Images were visualized and analyzed with an ECLIPSE Ti2 (Nikon) confocal laser scanning microscope.

## Statistics

Statistical significance was performed with GraphPad Prism. Differences between groups of mice were determined by one-way ANOVA with multiple comparisons.

## Results

### The first intron of *Foxn1* exhibits the characteristics of active REs

Promoter elements of *Foxn1* have been used previously to generate several transgenic animals (29–31). One transgene includes the 28kb region of DNA from the *Slc13a2* gene located 5' of the *Foxn1* promoter to the second exon of *Foxn1* (Fig. 1A, gray bar)(29). By reporter analysis, this transgene faithfully mimics endogenous *Foxn1* expression in TEC (29), indicating that regulatory elements directing *Foxn1* expression in TEC are likely to be located within this 28kb region.

We assessed chromatin accessibility, an indicator of active REs, using assay for transposase-accessible chromatin by sequencing (ATAC-Seq)(26). Standard ATAC-Seq protocols require only 50,000 cells making this a feasible method of testing chromatin characteristics in both cTEC and mTEC. We sorted TEC identified as EpCAM+CD45- and acquired a sufficient number of both cTEC (Ly51+UEA-1-) and mTEC (Ly51-UEA-1+) from embryonic stages (Fig. S1A). cTEC are difficult to isolate at post-natal stages and therefore only mTEC were used for ATAC-Seq at later stages (Fig. 1A)(32). We found that regions of accessible chromatin are present throughout the first intron of *Foxn1* (Fig. 1A). The 3' side of the intron (box "A") shows a large peak, indicating accessible chromatin, in embryonic stages of both cTEC and mTEC (Fig. 1A). The 5' side of the intron (box "B") contains a peak indicating accessible chromatin in mTEC (Fig. 1A).

We next compared results from ATAC-Seq to conserved elements identified by the PhastCons algorithm on the UCSC Genome Browser. Two conservation tracks (green) represent conservation across placental animals and vertebrates with peaks in the track indicating high levels of conservation (Fig. 1A). Each peak of accessible chromatin in the first intron of *Foxn1* corresponds to PhastCons elements further suggesting that critical REs are located in this region (Fig. 1A).

In addition, we examined previously published ChIP-Seq data for histone modifications generated from mTEC collected from 4–6-week-old mice (33). We examined H3K4me1 (enriched at poised and active enhancers), H3K27ac (enriched at active enhancers), and

H3K27me3 (linked to inactive gene expression) (24, 34). We found the first intron of *Foxn1* to be enriched for H3K4me1 and H3K27ac and devoid of signal for H3K27me3 in TECs (Fig. S2A). This epigenetic profile is indicative of active regulatory elements in the first intron of *Foxn1*.

CTCF binds to DNA and helps to form topologically associated domains (TADs). These TADs are characterized by enhanced interactions between loci within a TAD and help to facilitate enhancer-promoter interactions (35). CTCF ChIP-Seq data available from ENCODE/LICR through the UCSC Genome Browser shows consistent CTCF binding across many cell types at the *Foxn1* locus (Fig. S2B). Specifically, CTCF binding is located at the 5' end of the *Foxn1* gene and on the last exon of *Slc13a2*, the gene immediately 5' of *Foxn1* (Fig. S2B). This suggests that REs critical for *Foxn1* expression are located in close proximity to the *Foxn1* promoter.

### **Knockout of regions of the first intron of *Foxn1* severely disrupt thymus development, but cause no defects in the skin**

The previous observations together strongly suggested the presence of active REs within the first intron of *Foxn1*. This informed the generation of knockout animals by CRISPR/Cas9 in which each half of the first intron (shown as boxes labeled A and B) was deleted separately (Fig. 1A). The resulting homozygous knockout animals were designated *Foxn1*<sup>A/A</sup> or *Foxn1*<sup>B/B</sup> based on the region deleted (Fig. 1A). While total inactivation of *Foxn1* results in hairlessness exhibited by *Foxn1*<sup>nu/nu</sup> mice, both of the intron knockout mutants had a normal fur coat (Fig. 1B). Examination of the thymus, however, showed a striking phenotype as *Foxn1*<sup>A/A</sup> mice contained no apparent thymus, and appeared indistinguishable from *Foxn1*<sup>nu/nu</sup> mice in which *Foxn1* function is totally disrupted (Fig. 1C). Unlike the *Foxn1*<sup>A/A</sup> mouse, the *Foxn1*<sup>B/B</sup> mouse had no gross anatomical thymic defect (Fig. 1C).

Due to the apparent TEC specific phenotype of this knockout, we were curious if the *Foxn1* expressing cells of the hair follicles exhibited a chromatin accessibility landscape similar to TEC. *Foxn1* is expressed in the anagen (growth phase) portion of hair follicles and is not expressed in telogen (resting phase) hair follicles (36). We sorted CD45-Sca-1-EpCAM+ cells from the epidermis which contains the upper portion (isthmus) and the bulge region from telogen hair follicles (37), as well as from dissected anagen hair follicles, and examined chromatin accessibility by ATAC-Seq (Fig. 1D, Fig. S1B). Telogen hair follicle keratinocytes exhibited inaccessible chromatin in the first intron and promoter of *Foxn1* while anagen hair follicle keratinocytes showed accessible chromatin at the promoter; consistent with active gene expression (Fig. 1D). We found that unlike TEC, the first intron of *Foxn1* in hair follicle keratinocytes is not accessible (Fig. 1D). These data suggest that REs critical for *Foxn1* expression in hair follicle keratinocytes are not located in the first intron of *Foxn1*.

We also examined *Foxn1* expression by qRT-PCR with RNA extracted from sorted keratinocytes from the anagen portion of hair follicles. Consistent with normal hair growth, *Foxn1* expression was unchanged in *Foxn1*<sup>A/A</sup> mice compared to *Foxn1*<sup>+/+</sup> (Fig. 1E). These data show TEC specific regions of accessible chromatin in the first intron of *Foxn1*

that are critically important for the expression of *Foxn1* in the thymus, but unnecessary for *Foxn1* expression in the skin.

### ***Foxn1*<sup>A/A</sup> mice lack thymic function and do not generate T cells**

*Foxn1<sup>nu/nu</sup>* mice have an almost complete absence of peripheral T cells due to a maturational arrest of TEC development that renders the thymus unable to support T cell development (38). As a readout to determine if any thymic function remains in *Foxn1*<sup>A/A</sup> mice and to assess for potential functional thymic defects in *Foxn1*<sup>B/B</sup> mice, we examined peripheral T cell populations in the spleen (Fig. 2A and B). We assessed the abundance of T cells in the periphery by staining splenocytes with antibodies against TCRβ, CD4, and CD8 followed by flow cytometric analysis. In addition, we stained splenocytes for CD19 to identify extrathymic derived B cells as a control population that should be present in mice lacking a functional thymus. As predicted, numbers of CD19+ B cells in all mutants were not significantly different compared to *Foxn1<sup>+/+</sup>* controls (Fig. 2A). *Foxn1*<sup>A/A</sup> mice had almost no TCRβ+ T cells compared to *Foxn1<sup>+/+</sup>* mice (Fig. 2A). The loss of TCRβ+ cells in the *Foxn1*<sup>A/A</sup> mouse was as complete as that of the *Foxn1<sup>nu/nu</sup>* mouse by overall cell numbers (Fig. 2A). There was no change in the overall number of TCRβ+ cells in *Foxn1*<sup>B/B</sup> mice (Fig. 2A). Single-positive CD4+ (SP4) and CD8+ (SP8) cell proportions and cell numbers were normal in *Foxn1*<sup>B/B</sup> mice whereas SP4 and SP8 cells were nearly absent from *Foxn1*<sup>A/A</sup> mice (Fig. 2B).

### ***Foxn1*<sup>B/B</sup> mice have mild TEC defects, but have normal T cell populations**

There were no obvious gross anatomical thymus defects or changes in T cells in the periphery; however, we wanted to further examine the potential for TEC specific defects in *Foxn1*<sup>B/B</sup> mice. We found that *Foxn1*<sup>B/B</sup> mice had reduced overall TEC numbers (Fig. 3A). This reduction was specific to the mTEC population, with the number of cTEC in the *Foxn1*<sup>B/B</sup> mouse displaying a slight increase (Fig. 3B). We further examined the mTEC population of the *Foxn1*<sup>B/B</sup> mouse and found fewer MHCII+CD80+ (mTEChi) vs MHCIIIoCD80- (mTEClo) cells (Fig. 3C). This skewing in the frequency of mTEChi vs lo populations was due to a significant reduction in the numbers of mTEChi in the *Foxn1*<sup>B/B</sup> thymus, whilst mTEClo numbers remained unchanged compared to *Foxn1<sup>+/+</sup>* mice (Fig. 3C). We next examined *Foxn1* expression by qRT-PCR in sorted cTEC and mTEC from 6–8-week-old mice. *Foxn1* expression was unchanged in the cTEC of *Foxn1*<sup>B/B</sup> mice (Fig. 3D). Consistent with a loss of mTEC numbers, *Foxn1* expression was significantly lower in mTEC (Fig. 3D). This specific loss of MHCII+CD80+ mTEChi cells is consistent with previous reports of a hypomorphic phenotype resulting from reduced *Foxn1* expression in TEC (15).

To further investigate the loss of mTEC in *Foxn1*<sup>B/B</sup> mice we examined overall thymic architecture by immunofluorescent staining of cTEC by β5t and mTEC by UEA-I (Fig. 3E). Thymic architecture appeared normal, with well-defined boundaries between the cortex and medulla (Fig. 3E). As the *Foxn1*<sup>B/B</sup> thymus had a specific loss of mTEChi cells, which contain the Aire expressing mTEC (5), we examined if the *Foxn1*<sup>B/B</sup> mice had altered Aire expression. Confocal microscopy confirmed the presence and normal localization of Aire+ cells to medullary regions (Fig. 3E). Flow cytometric analysis revealed a significant



reduction in the frequency and number of Aire+ cells within the already reduced mTEChi mTEC population in *Foxn1*<sup>B/B</sup> mice (Fig. 3F).

We then examined if this significant loss of Aire+ mTEChi cells resulted in disruptions in T cell development in the thymus of *Foxn1*<sup>B/B</sup> mice. T cell precursors enter the thymus and begin to differentiate in the cortex. CD4-CD8- double-negative (DN) early thymic precursors (ETPs) progress through four stages of development before becoming CD4+CD8+ double-positive (DP) and migrating to the medulla. ETP (defined as Kit+CD25-CD4-CD8-TCRβ- lineage- (Lin-) whereby Lin- is the absence of TER119, CD11c, CD11b, CD19, B220, Gr1, Nk1.1, and Mac1), DN2 (Lin- TCRβ-Kit+CD25+), DN3 (Lin- TCRβ-Kit-CD25+), and DN4 (Lin- TCRβ-Kit-CD25-) cells showed no change in overall proportions or absolute cell number (Fig. 3G). We then examined the CD4 versus CD8 cell profile and found normal frequencies and numbers of DN, DP, SP4 and SP8 cells (Fig. 3H). We also examined CD5 expression on DP, SP4 and SP8 cells to assess TCR signaling intensity and found no difference between *Foxn1*<sup>B/B</sup> mice and *Foxn1*<sup>+/+</sup> mice (Fig. 3I) (39). Due to the loss of Aire+ mTEChi and the potential for autoimmune disease, we examined thymic Tregs. *Foxn1*<sup>B/B</sup> mice had normal populations of CD25+FoxP3+ Tregs by percentage and overall cell number (Fig. 3J). Thus, despite a significant reduction in the number of Aire+ mTEChi cells, we found no changes in the overall proportions or numbers of developing T cells, including Tregs, in the thymus; and no changes in the number of T cells in the periphery of *Foxn1*<sup>B/B</sup> mice.

#### A ~1.6kb region within the *Foxn1*<sup>A</sup> region is critical for thymus development

Our initial knockouts of the first intron of *Foxn1* removed very broad regions of DNA. Within the *Foxn1*<sup>A</sup> region, which is absolutely critical for thymus development, we identified multiple individual elements of accessible chromatin (Fig. 4A). We generated a new cohort of knockout mice based on the ATAC-Seq data in an effort to identify a specific region critical for *Foxn1* expression in TEC. Each element of accessible chromatin within the *Foxn1*<sup>A</sup> region was removed individually and we designated these *Foxn1*<sup>C</sup>, *Foxn1*<sup>D</sup>, and *Foxn1*<sup>E</sup> (Fig. 4A). Consistent with the *Foxn1*<sup>A/A</sup> mouse, all of these new mutant animals had normal fur coats (Fig. S3A). While the *Foxn1*<sup>C/C</sup> and *Foxn1*<sup>E/E</sup> mutants had a gross anatomically normal thymus, the *Foxn1*<sup>D/D</sup> mouse lacked a visible thymus (Fig. S3B).

We next wanted to further characterize the *Foxn1*<sup>D/D</sup> mouse to determine if disrupted thymus development and corresponding T cell defects were as severe as the *Foxn1*<sup>nu/nu</sup> mouse. Similar to *Foxn1*<sup>nu/nu</sup> and *Foxn1*<sup>A/A</sup> mice, *Foxn1*<sup>D/D</sup> mice contained almost no TCRβ+ T cells in the spleen (Fig. 4B). Quantification of absolute numbers of TCRβ+ cells showed no difference between the *Foxn1*<sup>nu/nu</sup> and *Foxn1*<sup>D/D</sup> mice, whereas overall numbers of CD19+ B cells were unchanged for all genotypes (Fig. 4B). The *Foxn1*<sup>C/C</sup> and *Foxn1*<sup>E/E</sup> mice were indistinguishable from *Foxn1*<sup>+/+</sup> mice and had normal populations of TCRβ+ cells in the spleen (Fig. 4B). *Foxn1*<sup>C/C</sup> and *Foxn1*<sup>E/E</sup> mice contained normal profiles and absolute numbers of TCRβ+ SP4 and SP8 cells compared to *Foxn1*<sup>+/+</sup> mice (Fig. 4C). *Foxn1*<sup>D/D</sup> mice had a near complete loss of SP4 and SP8 cells similar to *Foxn1*<sup>nu/nu</sup> mice (Fig. 4C).

Non-conventional T cell subsets are also dependent on the thymus for development (40–42) and we therefore examined these populations as further confirmation of loss of thymus function. Indeed, MAIT, NKT, V $\gamma$ 4+, and V $\gamma$ 6+ cells were absent in both the liver (Fig. 4D) and the lung (Fig. 4E) of *Foxn1*<sup>D/D</sup> mice. Therefore, the elements most critical for thymus development and subsequently T cell development in the *Foxn1*<sup>A</sup> region are located within the 1.6kb *Foxn1*<sup>D</sup> region.

In contrast to *Foxn1*<sup>nu/nu</sup> mice, *Foxn1*<sup>D/D</sup> mice have healthy body weights (Fig. S3C). *Foxn1*<sup>D/D</sup> mice are also born in normal Mendelian ratios (Fig. S3D). Overall, *Foxn1*<sup>D/D</sup> mice are more robust and easier to maintain than *Foxn1*<sup>nu/nu</sup> mice while still exhibiting thymic defects and T cell developmental defects as extreme as *Foxn1*<sup>nu/nu</sup> mice.

### ***Foxn1*<sup>C/C</sup> and *Foxn1*<sup>E/E</sup> mice do not have TEC or T cells defects**

Because of the severity of the *Foxn1*<sup>A/A</sup> mutation and the potential for mild TEC specific phenotypes such as in the *Foxn1*<sup>B/B</sup> mice, we further investigated the potential thymus phenotypes of the *Foxn1*<sup>C/C</sup> and *Foxn1*<sup>E/E</sup> mice. *Foxn1*<sup>C/C</sup> and *Foxn1*<sup>E/E</sup> mice had normal overall TEC numbers (Fig. S3E) and showed no difference in cTEC or mTEC numbers (Fig. S3F). *Foxn1*<sup>C/C</sup> and *Foxn1*<sup>E/E</sup> mice also had a normal profile of MHCIII<sup>lo</sup>CD80- mTEC<sup>lo</sup> and MHCIII<sup>hi</sup>CD80+ mTEC<sup>hi</sup> cells and normal numbers of mTEC<sup>hi</sup> and <sup>lo</sup> cells compared to *Foxn1*<sup>+/+</sup> mice (Fig. S3G).

To assess potential functional phenotypes, we examined T cell development in the thymus of the *Foxn1*<sup>C/C</sup> and *Foxn1*<sup>E/E</sup> mutants (Fig. S3H and S3I). There was no alteration of any DN stage cell population or overall numbers of each of the DN subtypes (Fig. S3H). Examination of total DN, and the more mature DP, SP4, and SP8 subsets showed that frequencies were the same as *Foxn1*<sup>+/+</sup> thymocytes and absolute cell numbers were also unchanged (Fig. S3I). These data show that the thymus phenotype resulting in the *Foxn1*<sup>A/A</sup> mice can be entirely attributed to the *Foxn1*<sup>D</sup> region of the first intron.

### ***Foxn1* expression is dramatically decreased in the *Foxn1*<sup>D/D</sup> embryonic thymus**

*Foxn1* expression can be detected by RT-PCR as early as E9.5 in the third pharyngeal pouch of the mouse embryo (8). We used a fluorescent *in situ* hybridization (FISH) method called RNAScope (ACDBio) to examine *Foxn1* expression in the developing embryo of *Foxn1*<sup>+/+</sup> control and intron knockout mice. We examined each mutant mouse at E11.5 and found fluorescent signal from RNA probes designed against *Foxn1* mRNA was readily detected in the *Foxn1*<sup>+/+</sup> control, *Foxn1*<sup>B/B</sup>, *Foxn1*<sup>C/C</sup>, and *Foxn1*<sup>E/E</sup> animals, whereas expression in the *Foxn1*<sup>D/D</sup> mutant embryo was almost completely absent (Fig. 5A). We also examined *Foxn1*<sup>+/+</sup> control and *Foxn1*<sup>D/D</sup> embryos at E10.5, soon after *Foxn1* is first expressed. *Foxn1* expression in the *Foxn1*<sup>+/+</sup> embryo was apparent throughout the epithelium but *Foxn1* expression was absent in the *Foxn1*<sup>D/D</sup> thymic bud (Fig. 5B). At E16.5, *Foxn1* expression was detected throughout both lobes of the thymus in the *Foxn1*<sup>+/+</sup> embryo; however, no *Foxn1* expression was detected in the *Foxn1*<sup>D/D</sup> embryonic thymus (Fig. 5C). The thymic buds were present but are greatly reduced in size (Fig. 5C). Overall, we detected little to no expression of *Foxn1* in the *Foxn1*<sup>D/D</sup> embryonic thymus and thymus development was severely disrupted by E16.5 in the *Foxn1*<sup>D/D</sup> mutant embryo.

## The *Foxn1* intronic RE is specific to *Foxn1* and functions in *cis*

To determine whether the intronic regulatory element functions in *cis* or *trans* we bred the *Foxn1*<sup>D/D</sup> mouse to the *Foxn1*<sup>nu/nu</sup>. The *Foxn1*<sup>nu/nu</sup> mutation is a single base pair substitution in the third exon that results in a nonsense mutation (Fig. 6A)(8). The first intron of the *Foxn1*<sup>nu/nu</sup> mouse is intact and the exons of the *Foxn1*<sup>D/D</sup> mouse are normal (Fig. 6A). If the RE functions in *trans*, the RE from the *nude* allele should be able to promote the expression of the *Foxn1* gene from the *Foxn1*<sup>D</sup> allele in the thymus. *Foxn1*<sup>D/nu</sup> mice have normal fur growth (Fig. 6B) but lack a normal thymus (Fig. 6C). We assessed peripheral T cell numbers by flow cytometry and found almost no TCRβ<sup>+</sup> cells in the spleen of *Foxn1*<sup>D/nu</sup> mouse and no difference in cell number between the *Foxn1*<sup>D/nu</sup>, *Foxn1*<sup>D/D</sup>, and *Foxn1*<sup>nu/nu</sup> mice (Fig. 6D). CD19<sup>+</sup> B cell numbers were unchanged in all mutants (Fig. 6D).

Altogether these data show that the *Foxn1*<sup>D</sup> regulatory element functions in *cis* and is specific to the regulation of *Foxn1* expression. The intact *Foxn1*<sup>D</sup> regulatory element on the *nude* allele is not sufficient or capable of functioning in *trans* to induce expression of *Foxn1* from the *Foxn1*<sup>D</sup> allele. Both the *Foxn1*<sup>D/+</sup> and *Foxn1*<sup>nu/+</sup> mice have a thymus and essentially normal T cell populations. Therefore, we would expect that if the *Foxn1*<sup>D</sup> mutation affected any other gene, possibly an upstream regulator of *Foxn1*, we would not see the thymus development phenotype observed in the *Foxn1*<sup>D/nu</sup> mouse. The *Foxn1*<sup>D</sup> mutation and the *Foxn1*<sup>nu</sup> mutation function in concert to totally disrupt *Foxn1* expression and function.

## Discussion

*Foxn1* is essential for the development of the thymus and ultimately, the adaptive immune system. Herein, we have identified the first genomic RE critical for *Foxn1* expression. This RE is remarkably tissue-specific as there is an almost total loss of expression of *Foxn1* in the thymic epithelium while leaving *Foxn1* expression and function in the skin unaffected. Loss of this RE results in defective thymus development and function and a near complete loss of T cells in the periphery. The *Foxn1*<sup>D</sup> RE is specific for *Foxn1* expression as shown by the *Foxn1*<sup>D/nu</sup> compound mutant mouse. The *Foxn1*<sup>B/B</sup> mouse identified a broader region of DNA containing a RE(s) specific for *Foxn1* expression in mTEC. However, this RE is significantly weaker than the *Foxn1*<sup>D</sup> RE and despite a reduction in the overall number of mTEChi cells, there were no identified T cell defects in the *Foxn1*<sup>B/B</sup> mouse.

We believe the *Foxn1*<sup>D/D</sup> mouse to be a good model to study thymus independent immune cell development. These animals are generally healthier than the *nude* mouse, breed like WT mice, and maintain *Foxn1* expression in the skin allowing for the study of immune cells that reside in the skin. The *Foxn1*<sup>D/D</sup> mice breed as homozygotes unlike the traditional *nude* mice which are known to have a poor capacity for breeding. This provides a robust and more easily accessible model to study thymus-related immunological questions.

Transcription factors can bind to the promoter, genomic regulatory elements, or both, to control gene expression. Studies have identified candidate regulators of *Foxn1* expression as several transcription factor knockouts result in mice lacking a functional thymus (6). *Pax*

family genes are expressed in the endoderm and knockout of *Pax1* results in a hypoplastic thymus while knockout of *Pax9* results in athymia (43, 44). Loss of *Hoxa3*, *Eya1*, or *Six1* results in severe thymic developmental defects (45–48). Signals from the surrounding endothelium and mesenchyme including *Bmp4* and Wnt signaling have been implicated in regulation of *Foxn1* expression (49, 50). While many of these factors have been implicated in *Foxn1* expression, none have been shown to directly bind to *Foxn1* REs to induce *Foxn1* expression in the early embryo. Several transcription factor binding motifs for Pax1, Six1, and Smads are present in the *Foxn1* first intron regulatory element (Fig. S4A); however, additional studies are needed to determine which of these transcription factors interact with this intronic element to promote *Foxn1* expression in TEC.

In humans, *FOXN1* mutations result in congenital alopecia, nail dystrophy and severe T cell lymphopenia (22). The *Foxn1<sup>D</sup>* RE exhibits a high level of sequence conservation with the human *FOXN1* intron. BLAT of the *Foxn1<sup>D</sup>* RE sequence to the human genome identifies a conserved region in the first intron of the *FOXN1* gene with 89.7% identity (UCSC Genome Browser BLAT). This suggests that the *Foxn1* RE we have identified in mouse could be critically important for *FOXN1* expression in human TEC.

Genome-wide association studies (GWAS) have shown that a large proportion of variants likely to cause human disease are located outside of the protein coding domains (51, 52). There is potential for this study to inform genomic screening assays for mutations in human *FOXN1* REs that currently remain undiagnosed. Whole exome sequencing and T cell receptor excision circle (TREC) count assays are performed on patients with T cell lymphopenia (53). It is likely that in some patients, *FOXN1* expression is disrupted due to mutations in the REs rather than the exons. Further study of this RE and its conserved human RE is therefore relevant for the proper identification and treatment of immunodeficiency disorders resulting from aberrant *FOXN1* expression in human patients.

## Supplementary Material

Refer to Web version on PubMed Central for supplementary material.

## Acknowledgements

We thank the CCR Sequencing Facility and CCR Flow Cytometry Core Facility for technical support; the NCI Pathology/Histotechnology Laboratory specifically Andrew Warner, Jennifer Matta, and Tamara Morgan; the Confocal Microscopy and Digital Imaging Core, Experimental Immunology Branch, National Cancer Institute specifically Jan Wisniewski; the Transgenics/Cryopreservation – Laboratory Animal Sciences Program; and the CCR Collaborative Bioinformatics group including Maggie Cam and Vishal Koparde.

This work was supported by the Intramural Research Program of the National Cancer Institute, Center for Cancer Research, National Institutes of Health.

## References

1. Shah DK, and Zuniga-Pflucker JC. 2014 An overview of the intrathymic intricacies of T cell development. *J Immunol* 192: 4017–4023. [PubMed: 24748636]
2. Cowan JE, Jenkinson WE, and Anderson G. 2015 Thymus medulla fosters generation of natural Treg cells, invariant gammadelta T cells, and invariant NKT cells: what we learn from intrathymic migration. *Eur J Immunol* 45: 652–660. [PubMed: 25615828]

3. Anderson G, and Jenkinson EJ. 2001 Lymphostromal interactions in thymic development and function. *Nat Rev Immunol* 1: 31–40. [PubMed: 11905812]
4. Manley NR, Richie ER, Blackburn CC, Condie BG, and Sage J. 2011 Structure and function of the thymic microenvironment. *Front Biosci (Landmark Ed)* 16: 2461–2477. [PubMed: 21622189]
5. Anderson G, and Takahama Y. 2012 Thymic epithelial cells: working class heroes for T cell development and repertoire selection. *Trends Immunol* 33: 256–263. [PubMed: 22591984]
6. Abramson J, and Anderson G. 2017 Thymic Epithelial Cells. *Annu Rev Immunol* 35: 85–118. [PubMed: 28226225]
7. Perry JSA, Lio CJ, Kau AL, Nutsch K, Yang Z, Gordon JI, Murphy KM, and Hsieh CS. 2014 Distinct contributions of Aire and antigen-presenting-cell subsets to the generation of self-tolerance in the thymus. *Immunity* 41: 414–426. [PubMed: 25220213]
8. Nehls M, Pfeifer D, Schorpp M, Hedrich H, and Boehm T. 1994 New member of the winged-helix protein family disrupted in mouse and rat nude mutations. *Nature* 372: 103–107. [PubMed: 7969402]
9. Nehls M, Kyewski B, Messerle M, Waldschutz R, Schuddekopf K, Smith AJ, and Boehm T. 1996 Two genetically separable steps in the differentiation of thymic epithelium. *Science* 272: 886–889. [PubMed: 8629026]
10. Pantelouris EM 1968 Absence of thymus in a mouse mutant. *Nature* 217: 370–371. [PubMed: 5639157]
11. Flanagan SP 1966 'Nude', a new hairless gene with pleiotropic effects in the mouse. *Genet Res* 8: 295–309. [PubMed: 5980117]
12. Bennett AR, Farley A, Blair NF, Gordon J, Sharp L, and Blackburn CC. 2002 Identification and characterization of thymic epithelial progenitor cells. *Immunity* 16: 803–814. [PubMed: 12121662]
13. Alves NL, Takahama Y, Ohigashi I, Ribeiro AR, Baik S, Anderson G, and Jenkinson WE. 2014 Serial progression of cortical and medullary thymic epithelial microenvironments. *Eur J Immunol* 44: 16–22. [PubMed: 24214487]
14. Bleul CC, Corbeaux T, Reuter A, Fisch P, Monting JS, and Boehm T. 2006 Formation of a functional thymus initiated by a postnatal epithelial progenitor cell. *Nature* 441: 992–996. [PubMed: 16791198]
15. Zuklys S, Handel A, Zhanybekova S, Govani F, Keller M, Maio S, Mayer CE, Teh HY, Hafen K, Gallone G, Barthlott T, Ponting CP, and Hollander GA. 2016 Foxn1 regulates key target genes essential for T cell development in postnatal thymic epithelial cells. *Nat Immunol* 17: 1206–1215. [PubMed: 27548434]
16. Chen L, Xiao S, and Manley NR. 2009 Foxn1 is required to maintain the postnatal thymic microenvironment in a dosage-sensitive manner. *Blood* 113: 567–574. [PubMed: 18978204]
17. Corbeaux T, Hess I, Swann JB, Kanzler B, Haas-Assenbaum A, and Boehm T. 2010 Thymopoiesis in mice depends on a Foxn1-positive thymic epithelial cell lineage. *Proc Natl Acad Sci U S A* 107: 16613–16618. [PubMed: 20823228]
18. Cheng L, Guo J, Sun L, Fu J, Barnes PF, Metzger D, Chambon P, Oshima RG, Amagai T, and Su DM. 2010 Postnatal tissue-specific disruption of transcription factor FoxN1 triggers acute thymic atrophy. *J Biol Chem* 285: 5836–5847. [PubMed: 19955175]
19. Sun L, Guo J, Brown R, Amagai T, Zhao Y, and Su DM. 2010 Declining expression of a single epithelial cell-autonomous gene accelerates age-related thymic involution. *Aging Cell* 9: 347–357. [PubMed: 20156205]
20. Zook EC, Krishack PA, Zhang S, Zeleznik-Le NJ, Firulli AB, Witte PL, and Le PT. 2011 Overexpression of Foxn1 attenuates age-associated thymic involution and prevents the expansion of peripheral CD4 memory T cells. *Blood* 118: 5723–5731. [PubMed: 21908422]
21. Bredenkamp N, Nowell CS, and Blackburn CC. 2014 Regeneration of the aged thymus by a single transcription factor. *Development* 141: 1627–1637. [PubMed: 24715454]
22. Adriani M, Martinez-Mir A, Fusco F, Busiello R, Frank J, Telese S, Matrecano E, Ursini MV, Christiano AM, and Pignata C. 2004 Ancestral founder mutation of the nude (FOXN1) gene in congenital severe combined immunodeficiency associated with alopecia in southern Italy population. *Ann Hum Genet* 68: 265–268. [PubMed: 15180707]

23. Visel A, Blow MJ, Li Z, Zhang T, Akiyama JA, Holt A, Plajzer-Frick I, Shoukry M, Wright C, Chen F, Afzal V, Ren B, Rubin EM, and Pennacchio LA. 2009 ChIP-seq accurately predicts tissue-specific activity of enhancers. *Nature* 457: 854–858. [PubMed: 19212405]
24. Creighton MP, Cheng AW, Welstead GG, Kooistra T, Carey BW, Steine EJ, Hanna J, Lodato MA, Frampton GM, Sharp PA, Boyer LA, Young RA, and Jaenisch R. 2010 Histone H3K27ac separates active from poised enhancers and predicts developmental state. *Proc Natl Acad Sci U S A* 107: 21931–21936. [PubMed: 21106759]
25. Noonan JP, and McCallion AS. 2010 Genomics of long-range regulatory elements. *Annu Rev Genomics Hum Genet* 11: 1–23. [PubMed: 20438361]
26. Buenrostro JD, Giresi PG, Zaba LC, Chang HY, and Greenleaf WJ. 2013 Transposition of native chromatin for fast and sensitive epigenomic profiling of open chromatin, DNA-binding proteins and nucleosome position. *Nat Methods* 10: 1213–1218. [PubMed: 24097267]
27. Heinz S, Benner C, Spann N, Bertolino E, Lin YC, Laslo P, Cheng JX, Murre C, Singh H, and Glass CK. 2010 Simple combinations of lineage-determining transcription factors prime cis-regulatory elements required for macrophage and B cell identities. *Mol Cell* 38: 576–589. [PubMed: 20513432]
28. Murata S, Sasaki K, Kishimoto T, Niwa S, Hayashi H, Takahama Y, and Tanaka K. 2007 Regulation of CD8+ T cell development by thymus-specific proteasomes. *Science* 316: 1349–1353. [PubMed: 17540904]
29. Bleul CC, and Boehm T. 2005 BMP signaling is required for normal thymus development. *J Immunol* 175: 5213–5221. [PubMed: 16210626]
30. Cunliffe VT, Furlley AJ, and Keenan D. 2002 Complete rescue of the nude mutant phenotype by a wild-type *Foxn1* transgene. *Mamm Genome* 13: 245–252. [PubMed: 12016512]
31. Kurooka H, Segre JA, Hirano Y, Nemhauser JL, Nishimura H, Yoneda K, Lander ES, and Honjo T. 1996 Rescue of the hairless phenotype in nude mice by transgenic insertion of the wild-type *Hfh11* genomic locus. *Int Immunol* 8: 961–966. [PubMed: 8671685]
32. Sakata M, Ohigashi I, and Takahama Y. 2018 Cellularity of Thymic Epithelial Cells in the Postnatal Mouse. *J Immunol* 200: 1382–1388. [PubMed: 29298829]
33. Bansal K, Yoshida H, Benoist C, and Mathis D. 2017 The transcriptional regulator Aire binds to and activates super-enhancers. *Nat Immunol* 18: 263–273. [PubMed: 28135252]
34. Heintzman ND, Stuart RK, Hon G, Fu Y, Ching CW, Hawkins RD, Barrera LO, Van Calcar S, Qu C, Ching KA, Wang W, Weng Z, Green RD, Crawford GE, and Ren B. 2007 Distinct and predictive chromatin signatures of transcriptional promoters and enhancers in the human genome. *Nat Genet* 39: 311–318. [PubMed: 17277777]
35. Dixon JR, Selvaraj S, Yue F, Kim A, Li Y, Shen Y, Hu M, Liu JS, and Ren B. 2012 Topological domains in mammalian genomes identified by analysis of chromatin interactions. *Nature* 485: 376–380. [PubMed: 22495300]
36. Lee D, Prowse DM, and Brissette JL. 1999 Association between mouse nude gene expression and the initiation of epithelial terminal differentiation. *Dev Biol* 208: 362–374. [PubMed: 10191051]
37. Nagao K, Kobayashi T, Moro K, Ohyama M, Adachi T, Kitashima DY, Ueha S, Horiuchi K, Tanizaki H, Kabashima K, Kubo A, Cho YH, Clausen BE, Matsushima K, Suematsu M, Furtado GC, Lira SA, Farber JM, Udey MC, and Amagai M. 2012 Stress-induced production of chemokines by hair follicles regulates the trafficking of dendritic cells in skin. *Nat Immunol* 13: 744–752. [PubMed: 22729248]
38. Blackburn CC, Augustine CL, Li R, Harvey RP, Malin MA, Boyd RL, Miller JF, and Morahan G. 1996 The *nu* gene acts cell-autonomously and is required for differentiation of thymic epithelial progenitors. *Proc Natl Acad Sci U S A* 93: 5742–5746. [PubMed: 8650163]
39. Azzam HS, Grinberg A, Lui K, Shen H, Shores EW, and Love PE. 1998 CD5 expression is developmentally regulated by T cell receptor (TCR) signals and TCR avidity. *J Exp Med* 188: 2301–2311. [PubMed: 9858516]
40. Tilloy F, Treiner E, Park SH, Garcia C, Lemonnier F, de la Salle H, Bendelac A, Bonneville M, and Lantz O. 1999 An invariant T cell receptor alpha chain defines a novel TAP-independent major histocompatibility complex class Ib-restricted alpha/beta T cell subpopulation in mammals. *J Exp Med* 189: 1907–1921. [PubMed: 10377186]

41. Benlagha K, Wei DG, Veiga J, Teyton L, and Bendelac A. 2005 Characterization of the early stages of thymic NKT cell development. *J Exp Med* 202: 485–492. [PubMed: 16087715]
42. Fahl SP, Coffey F, and Wiest DL. 2014 Origins of gammadelta T cell effector subsets: a riddle wrapped in an enigma. *J Immunol* 193: 4289–4294. [PubMed: 25326547]
43. Wallin J, Eibel H, Neubuser A, Wilting J, Koseki H, and Balling R. 1996 Pax1 is expressed during development of the thymus epithelium and is required for normal T-cell maturation. *Development* 122: 23–30. [PubMed: 8565834]
44. Peters H, Neubuser A, Kratochwil K, and Balling R. 1998 Pax9-deficient mice lack pharyngeal pouch derivatives and teeth and exhibit craniofacial and limb abnormalities. *Genes Dev* 12: 2735–2747. [PubMed: 9732271]
45. Zou D, Silvius D, Davenport J, Grifone R, Maire P, and Xu PX. 2006 Patterning of the third pharyngeal pouch into thymus/parathyroid by Six and Eya1. *Dev Biol* 293: 499–512. [PubMed: 16530750]
46. Xu PX, Zheng W, Laclef C, Maire P, Maas RL, Peters H, and Xu X. 2002 Eya1 is required for the morphogenesis of mammalian thymus, parathyroid and thyroid. *Development* 129: 3033–3044. [PubMed: 12070080]
47. Manley NR, and Capecchi MR. 1995 The role of Hoxa-3 in mouse thymus and thyroid development. *Development* 121: 1989–2003. [PubMed: 7635047]
48. Manley NR, and Capecchi MR. 1998 Hox group 3 paralogs regulate the development and migration of the thymus, thyroid, and parathyroid glands. *Dev Biol* 195: 1–15. [PubMed: 9520319]
49. Wertheimer T, Velardi E, Tsai J, Cooper K, Xiao S, Kloss CC, Ottmuller KJ, Mokhtari Z, Brede C, deRoos P, Kinsella S, Palikuqi B, Ginsberg M, Young LF, Kreines F, Lieberman SR, Lazrak A, Guo P, Malard F, Smith OM, Shono Y, Jenq RR, Hanash AM, Nolan DJ, Butler JM, Beilhack A, Manley NR, Rafii S, Dudakov JA, and van den Brink MRM. 2018 Production of BMP4 by endothelial cells is crucial for endogenous thymic regeneration. *Sci Immunol* 3.
50. Balcunaite G, Keller MP, Balcunaite E, Piali L, Zuklys S, Mathieu YD, Gill J, Boyd R, Sussman DJ, and Hollander GA. 2002 Wnt glycoproteins regulate the expression of FoxN1, the gene defective in nude mice. *Nat Immunol* 3: 1102–1108. [PubMed: 12379851]
51. Rickels R, and Shilatifard A. 2018 Enhancer Logic and Mechanics in Development and Disease. *Trends Cell Biol* 28: 608–630. [PubMed: 29759817]
52. Sakabe NJ, Savic D, and Nobrega MA. 2012 Transcriptional enhancers in development and disease. *Genome Biol* 13: 238. [PubMed: 22269347]
53. Kwan A, Abraham RS, Currier R, Brower A, Andruszewski K, Abbott JK, Baker M, Ballow M, Bartoshesky LE, Bonilla FA, Brokopp C, Brooks E, Caggana M, Celestin J, Church JA, Comeau AM, Connelly JA, Cowan MJ, Cunningham-Rundles C, Dasu T, Dave N, De La Morena MT, Duffner U, Fong CT, Forbes L, Freedenberg D, Gelfand EW, Hale JE, Hanson IC, Hay BN, Hu D, Infante A, Johnson D, Kapoor N, Kay DM, Kohn DB, Lee R, Lehman H, Lin Z, Lorey F, Abdel-Mageed A, Manning A, McGhee S, Moore TB, Naides SJ, Notarangelo LD, Orange JS, Pai SY, Porteus M, Rodriguez R, Romberg N, Routes J, Ruehle M, Rubenstein A, Saavedra-Matiz CA, Scott G, Scott PM, Secord E, Seroogy C, Shearer WT, Siegel S, Silvers SK, Stiehm ER, Sugerman RW, Sullivan JL, Tanksley S, Tierce M. L. t., Verbsky J, Vogel B, Walker R, Walkovich K, Walter JE, Wasserman RL, Watson MS, Weinberg GA, Weiner LB, Wood H, Yates AB, Puck JM, and Bonagura VR. 2014 Newborn screening for severe combined immunodeficiency in 11 screening programs in the United States. *JAMA* 312: 729–738. [PubMed: 25138334]

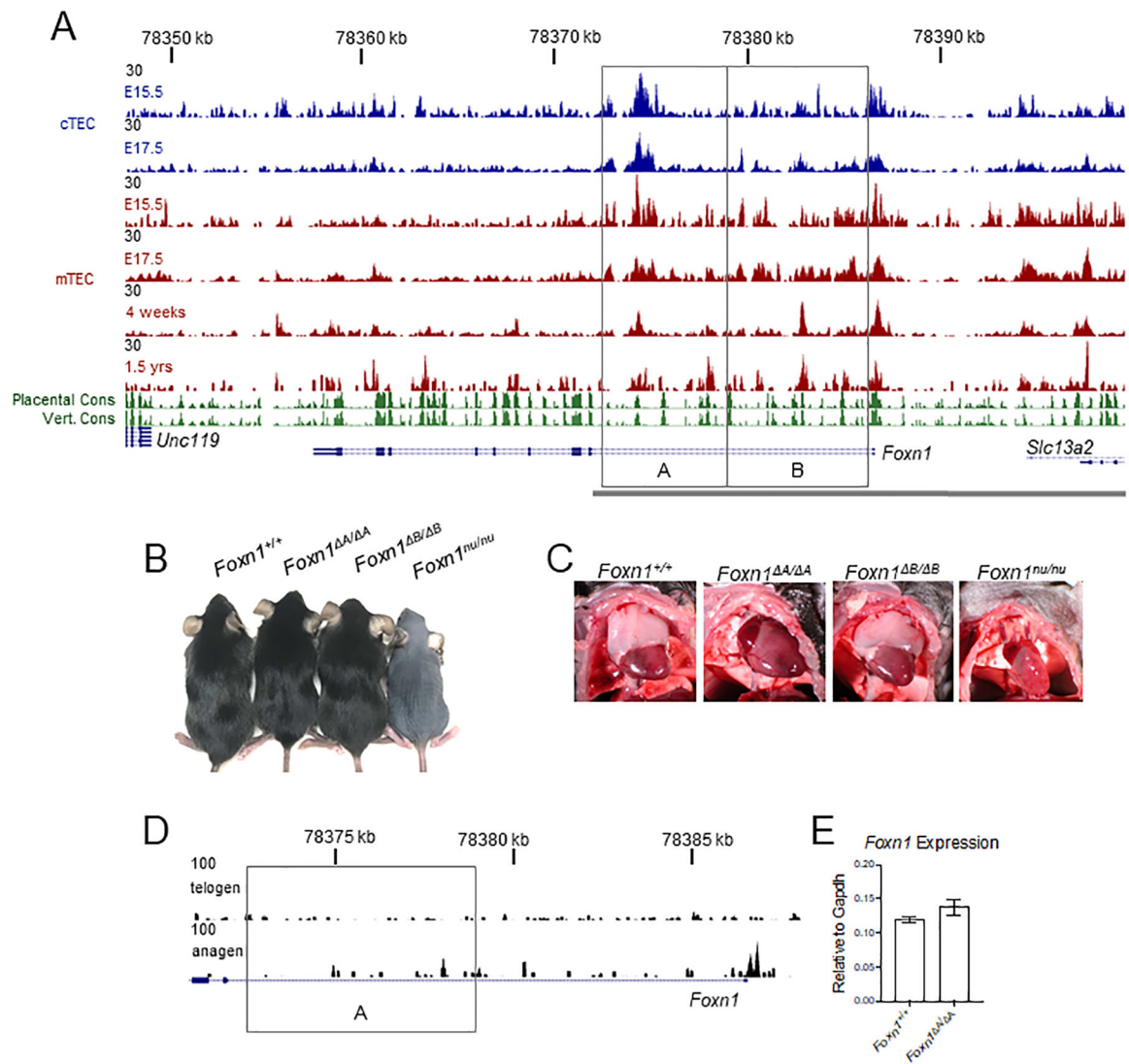
**Key Points**

Regulatory elements critical for *Foxn1* expression are in the first intron of *Foxn1*.

These elements are necessary for *Foxn1* expression in thymic epithelial cells.

These elements are not required for *Foxn1* expression in the skin.



**Figure 1.**

TEC specific chromatin accessibility identifies a functional regulatory element. (A) 50,000 cTEC (CD45-EpCAM+Ly51+UEA-1-) and mTEC (CD45-EpCAM+Ly51-UEA-1+) were sorted for ATAC-Seq at the indicated ages. Conservation (PhastCons) tracks of placental and vertebrate animals are shown from the UCSC Genome Browser. Knockouts of the first intron were done by CRISPR-Cas9. The resulting knockouts are indicated by the gray boxes and regions are identified as A and B. Mice resulting from the deletion of the A or B regions were designated *Foxn1*<sup>A</sup> and *Foxn1*<sup>B</sup> respectively. The gray bar represents the 28kb of DNA used to drive reporter expression in TECs in a previously described transgenic mouse (29). (B) Gross fur coat morphology of intron knockouts aged 6–8 weeks and *Foxn1*<sup>nu/nu</sup> mice. (C) Images of the thymus of intron knockout mice and the *Foxn1*<sup>nu/nu</sup> mouse. (D) 50,000 cells from the hair follicle (CD45-Sca-1-EpCAM+) were sorted for ATAC-Seq. The gray box indicates the deleted region in the *Foxn1*<sup>A/A</sup> mouse. (E) *Foxn1* expression in sorted hair follicle cells in anagen (4–5wk old mice) was measured by qRT-PCR. The bar

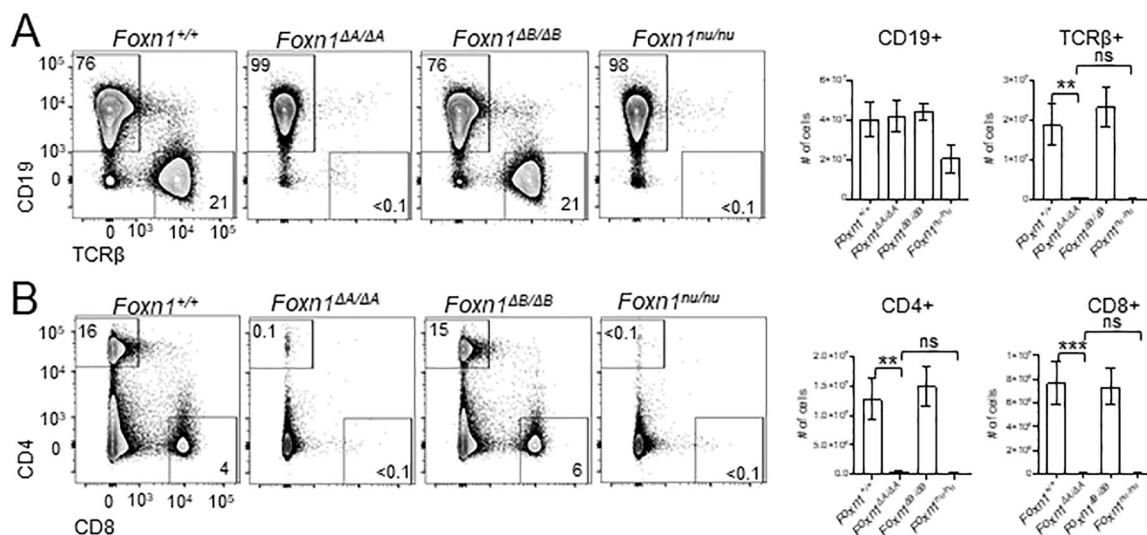
plot represents mean  $\pm$  SEM for  $n = 3-4$  mice per genotype. ANOVA was performed to determine statistical significance.

Author Manuscript

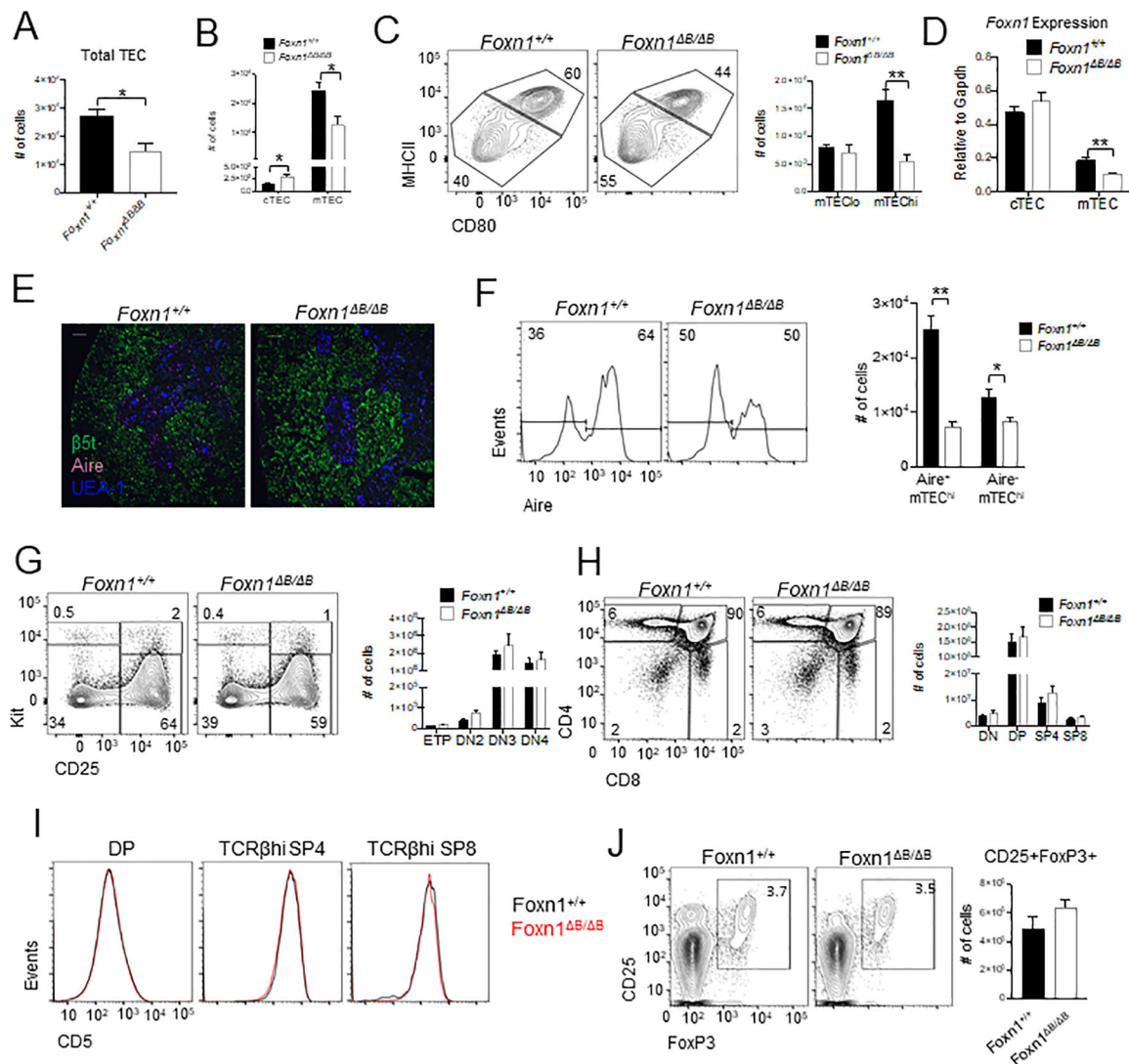
Author Manuscript

Author Manuscript

Author Manuscript



**Figure 2.** *Foxn1*<sup>A/A</sup> mice lack T cells. Flow cytometry was used to analyze T cell populations in the spleen as a readout of thymus function. (A) Representative flow cytometry plots of Lin-splenocytes comparing intron knockout mice to *Foxn1*<sup>nu/nu</sup> mice. Numbers show the percentage of cells in each gate. Total numbers of CD19+ cells and TCRβ+ cells per spleen calculated from DAPI- live cells. (B) Representative flow cytometry plots showing DAPI-Lin- CD4+ and CD8+ populations in the spleen. Total number of CD4+ and CD8+ cells per spleen was calculated from DAPI- live cells. All bar plots show mean ± SEM for *n* = 4–7 mice (5–8 weeks old) per genotype. ANOVA was performed to determine statistical significance. \*\* *p* < 0.01, \*\*\* *p* < 0.001.

**Figure 3.**

*Foxn1*<sup>B/B</sup> mice have mild mTEC defects but no apparent defect in T cell populations or cell numbers. Absolute numbers of total TEC (A) and cTEC and mTEC (B). (C) Representative flow plots of CD45-EpCAM+Ly51-UEA-1+ gated mTECs showing MHCIIhiCD80+ mTEChi vs MHCIIloCD80- mTEClo and calculations of overall cell numbers. (D) EpCAM+CD45- cTEC (Ly51+UEA-1-) and mTEC (Ly51-UEA-1-) were sorted and *Foxn1* expression was measured by qRT-PCR. (E) Immunofluorescence analysis of thymic sections from indicated mice for β5t (green), Aire (magenta), and UEA-1 (blue). Scale bars indicate 100 μm. (F) Flow cytometry analysis of Aire expression in mTEChi (EpCAM+CD45-UEA-1+Ly51-MHCIIhiCD80+). (G) Lin-TCRβ-CD4-CD8- gated representative flow cytometry plots and overall cell numbers for ETPs (Kit<sup>hi</sup>CD25-), DN2 (Kit<sup>hi</sup>CD25+), DN3 (Kit-CD25+), and DN4 (Kit-CD25-). (H) Lin- gated thymocytes showing CD4 and CD8 profiles and overall cell numbers for each population. (I) Flow cytometry of thymocytes showing CD5 expression on DAPI- DP, TCRβhi SP4 and TCRβhi SP8 cells (J) Flow cytometry analysis and quantification of Tregs (CD4+CD8-TCRβ

+CD25+FoxP3+) in the thymus. All bar plots show mean  $\pm$  SEM for  $n = 4-7$  mice (6-8 weeks old) per genotype. ANOVA was performed to determine statistical significance. \* $p < 0.05$ , \*\* $p < 0.01$ .

Author Manuscript

Author Manuscript

Author Manuscript

Author Manuscript

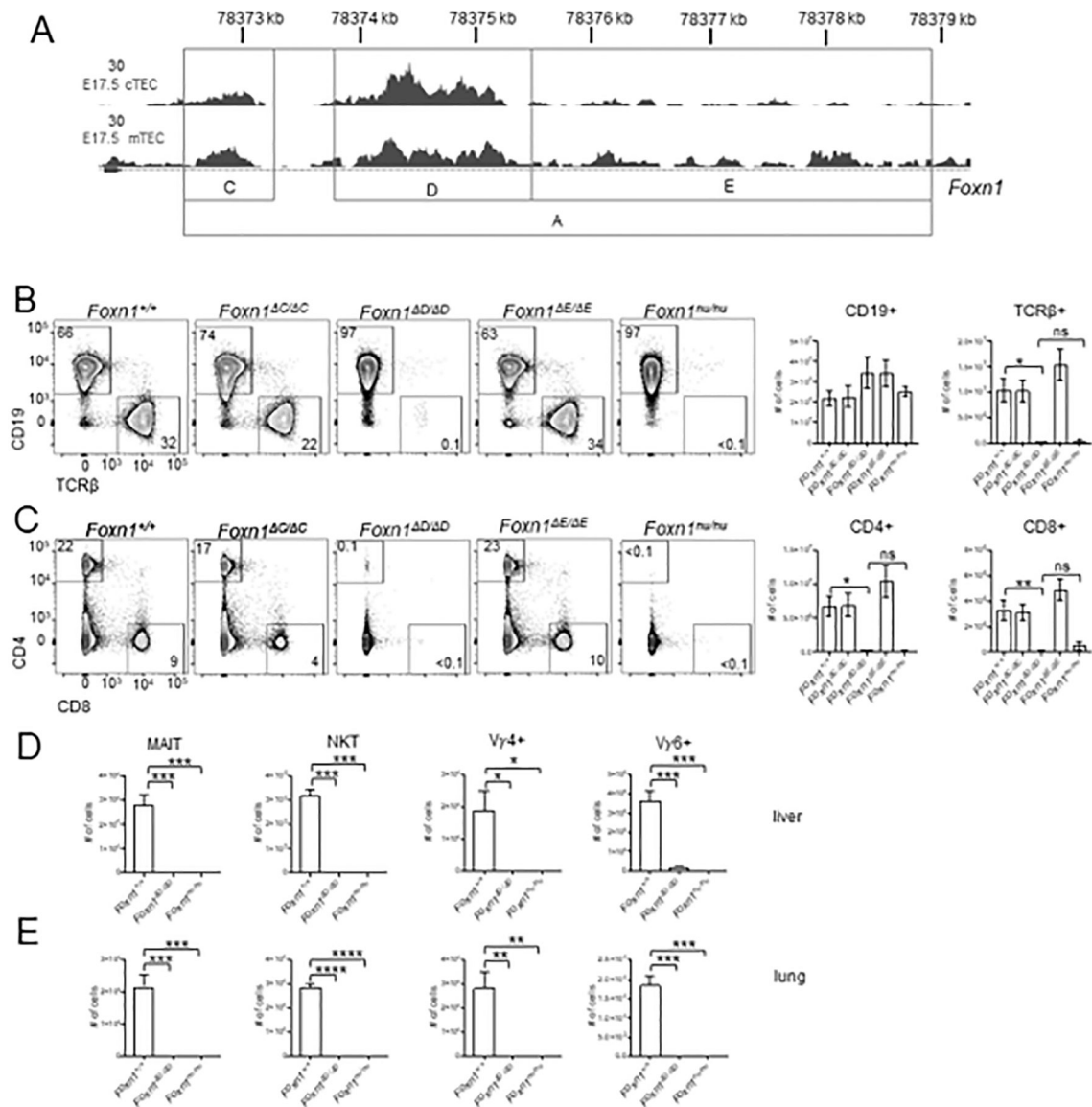


**Figure 4.**

*Foxn1*<sup>D/D</sup> mice have severely reduced T cells in the periphery. (A) gRNAs were designed to target potential regulatory elements within the A region of the first intron identified by ATAC-Seq. ATAC-Seq data shown is of E17.5 cTEC and mTEC. The gray boxes indicate regions that were deleted within the A region. The resulting mice were designated *Foxn1*<sup>C</sup>, *Foxn1*<sup>D</sup>, and *Foxn1*<sup>E</sup>. (B) Representative flow cytometry plots showing Lin<sup>-</sup> gated CD19<sup>+</sup> B cells and TCRβ<sup>+</sup> T cells from the spleen. Total cell numbers were calculated from all DAPI<sup>-</sup> live cells per spleen. (C) Flow cytometric analysis of DAPI-Lin<sup>-</sup> CD4<sup>+</sup> and CD8<sup>+</sup> cells in the spleen. Total cell numbers were calculated from DAPI<sup>-</sup> live cells. Absolute cell numbers in the liver (D) and lung (E) of MAIT cells (CD45<sup>+</sup>Thy1.2<sup>+</sup>TCRγδ<sup>+</sup>TCRβ<sup>+</sup>+mMR1 5-OP-RU tetramer<sup>+</sup>), NKT (CD45<sup>+</sup>Thy1.2<sup>+</sup> TCRγδ<sup>+</sup>TCRβ<sup>+</sup>+mCD1dPBS57 tetramer<sup>+</sup>), and γδ T cell populations (CD45<sup>+</sup>Thy1.2<sup>+</sup> TCRγδ<sup>+</sup>RORγt<sup>+</sup>) Vγ4<sup>+</sup> and Vγ6<sup>+</sup> (CD45<sup>+</sup>Thy1.2<sup>+</sup> TCRγδ<sup>+</sup>RORγt<sup>+</sup> Vγ4<sup>-</sup>). All absolute cell counts are shown as mean ±

SEM for  $n = 3-8$  mice (4-8 weeks old) per genotype. ANOVA was performed to determine statistical significance. \* $p < 0.05$ , \*\* $p < 0.01$ , \*\*\* $p < 0.001$ , \*\*\*\* $p < 0.0001$ .

Author Manuscript

Author Manuscript

Author Manuscript

Author Manuscript

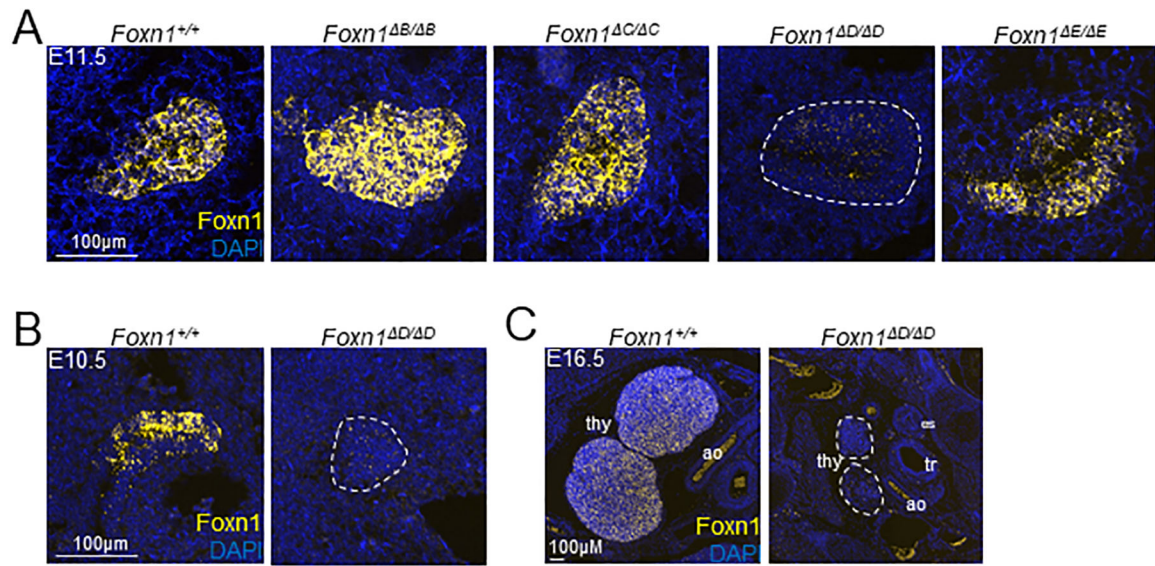


**Figure 5.**

*Foxn1* expression is absent in the *Foxn1*<sup>D/D</sup> embryonic thymus. *Foxn1* mRNA was visualized using fluorescent *in situ* hybridization. (A) Sagittal sections were taken of E11.5 embryos for each genotype. (B) Sagittal sections were taken of E10.5 control and *Foxn1*<sup>D/D</sup> embryos. (C) Transverse sections were taken of E16.5 embryos. ao = aorta, tr = trachea, es = esophagus. White dotted outline indicates the thymus in *Foxn1*<sup>D/D</sup> mice.



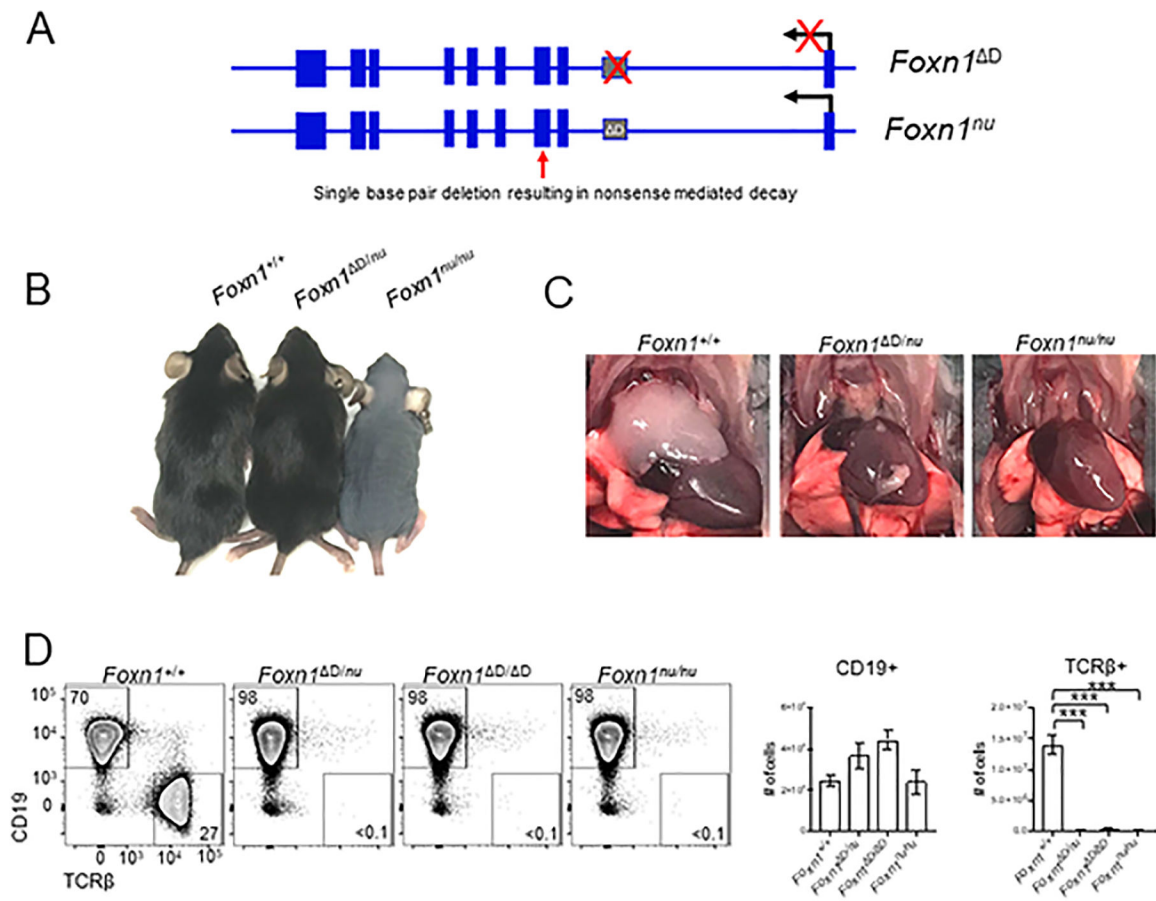


**Figure 6.**

The *Foxn1*<sup>D</sup> RE is specific to *Foxn1* and functions in *cis*. (A) Comparison of the mutations of the *Foxn1* gene in *Foxn1*<sup>D/D</sup> and *Foxn1*<sup>nu/nu</sup> mice. (B) Images of *Foxn1*<sup>+/+</sup>, *Foxn1*<sup>D/nu</sup>, and *Foxn1*<sup>nu/nu</sup> mice showing normal overall fur coat in the *Foxn1*<sup>D/nu</sup> mouse. (C) The *Foxn1*<sup>D/nu</sup> mouse lacks a normal appearing thymus just like the *Foxn1*<sup>nu/nu</sup> mouse. (D) Flow cytometric analysis was used to examine TCRβ<sup>+</sup> cells in the spleen. Total cell numbers were calculated from DAPI<sup>-</sup> cells. There is a significant loss of TCRβ<sup>+</sup> cells in the *Foxn1*<sup>D/nu</sup> mouse however there is no difference in the overall number of TCRβ<sup>+</sup> cells in the *Foxn1*<sup>D/nu</sup> mouse compared to the *Foxn1*<sup>D/D</sup> and *Foxn1*<sup>nu/nu</sup> mice. Total cell numbers were calculated from DAPI<sup>-</sup> live cells and shown as mean ± SEM for *n* = 3–4 mice (4–8 weeks old) per genotype. ANOVA was performed to determine statistical significance. \*\*\* *p* < 0.001.